

Model test on slope deformation and failure caused by transition from open-pit to underground mining

Bin Zhang^{1a}, Hanxun Wang^{1b}, Jie Huang^{*2} and Nengxiong Xu^{1c}

¹*School of Engineering and Technology, China University of Geosciences (Beijing),
29 Xueyuan Road, Haidian District, Beijing 100083, China*

²*Department of Civil and Environmental Engineering, The University of Texas at San Antonio,
1 UTSA Circle, San Antonio, Texas, 78249, U.S.A.*

(Received October 4, 2018, Revised September 29, 2019, Accepted September 30, 2019)

Abstract. Open-pit (OP) and underground (UG) mining are usually used to exploit shallow and deep ore deposits, respectively. When mine deposit starts from shallow subsurface and extends to a great depth, sequential use of OP and UG mining is an efficient and economical way to maintain mining productivity. However, a transition from OP to UG mining could induce significant rock movements that cause the slope instability of the open pit. Based on Yanqianshan Iron Mine, which was in the transition from OP to UG mining, a large-scale two-dimensional (2D) model test was built according to the similar theory. Thereafter, the UG mining was carried out to mimic the process of transition from OP to UG mining to disclose the triggered rock movement as well as to assess the associated slope instability. By jointly using three-dimensional (3D) laser scanning, distributed fiber optics, and digital photogrammetry measurement, the deformations, movements and strains of the rock slope during mining were monitored. The obtained data showed that the transition from OP to UG mining led to significant slope movements and deformations that can trigger catastrophic slope failure. The progressive movement of the slope could be divided into three stages: onset of micro-fracture, propagation of tensile cracks, and the overturning and/or sliding of slopes. The failure mode depended on the orientation of structural joints of the rock mass as well as the formation of tension cracks. This study also proved that these non-contact monitoring technologies were valid methods to acquire the interior strain and external deformation with high precision.

Keywords: open-pit mining; underground mining; similar theory; 3D laser scanning technology; distributed optic fiber; slope failure

1. Introduction

Normally, Open-pit (OP) mining is a preferred mining method in most circumstances, especially for shallow ore mineral deposits, due to its applicability to a variety of rocks, minimum production loss and high production rate (Korkmaz *et al.* 2011, Song *et al.* 2016). Due to these advantages, OP mining is the primary mining method in China for decades. However, some deposits start from shallow subsurface and extend to a great depth, which usually require a transition from OP to underground (UG) mining to maintain the productivity because the sloping of OP mining reduces the mining area with depth (Bakhtavar *et al.* 2009, Chung *et al.* 2016, Nguyen *et al.* 2016). Therefore, such mining usually will experience three production phases over its service life, namely, OP mining

at its early phase, combination of OP and UG mining at its interim phase and UG mining at its late phase. From an economic point of view, many studies have investigated the suitability, the optimal operation and the optimal transition depth from OP to UG, and have proposed many empirical models (Bakhtavar *et al.* 2013, Ordin *et al.* 2014). One of the greatest challenges of transition from OP to UG mining is the slope instability associated with high, steep cut and, in addition, the mining disturbance significantly increases the complexity (Bye *et al.* 2001, Rose *et al.* 2007, He *et al.* 2008). In the OP and UG mining concurrent phase, UG mining leads to stress redistribution of the OP slope, which may cause excessive movements, resulting in instability or even collapse in the long term (Chung *et al.* 2016). Therefore, the deformation and stability of the slope during the transition from OP to UG mining has been a key technical issue that was mainly investigated by numerical approaches in the past because a full-scale experimental test was prohibitive due to its high cost and space requirement.

Physical model tests can be a good alternative to simulate the problem in a lab environment if a prototype can be reasonably scaled down based on the similar theory. After first proposed by Genn Kuznetsov in the 1930s, the similar theory has established its mathematical basis to scale down a real-world project into an accommodable size to be tested in the lab. It has been widely applied in many

*Corresponding author, Associate Professor

E-mail: jie.huang@utsa.edu

^aAssociate Professor

E-mail: sc_zhb@cugb.edu.cn

^bPh.D.

E-mail: w_hanxun@cugb.edu.cn

^cProfessor

E-mail: xunengxiong@cugb.edu.cn

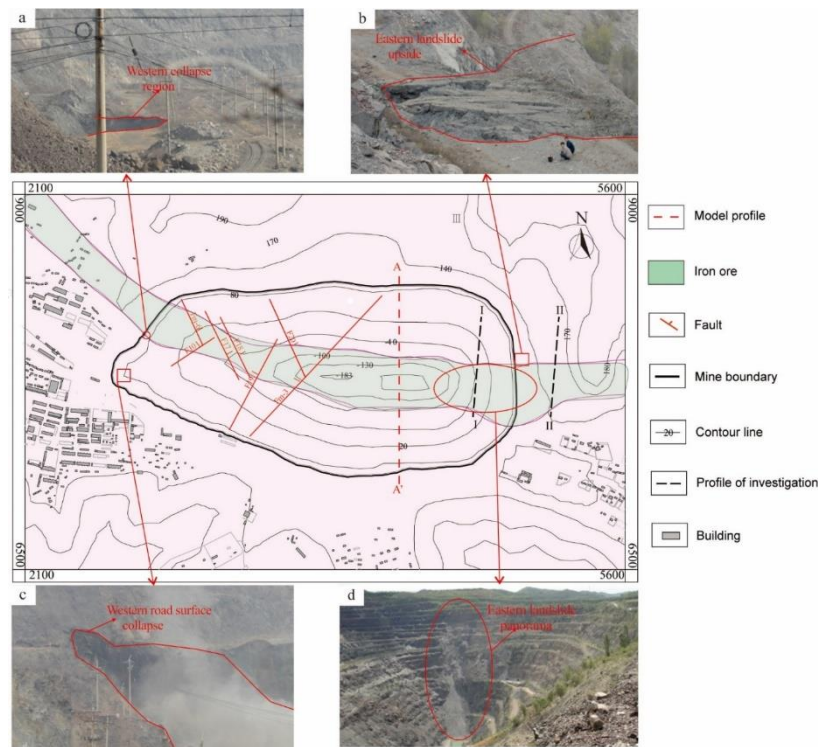


Fig. 1 Yanqianshan Iron Mine open pit

different areas, such as infrastructure, mining, fluid dynamics, aerospace, petroleum engineering and manufacturing. In 1973, based on the similar theory Fumagalli *et al.* (1973) first systematically performed a number of model tests to study different geomechanic problems and demonstrated how to establish the similarity between the in-situ materials and laboratory materials (i.e., similar materials), and how to apply stresses in model tests. With the encouraging success, model tests have been widely used in slope, tunneling and, mining engineering and become an indispensable tool for many engineering problems (Gu *et al.* 2008, Wang *et al.* 2014, Lin *et al.* 2015, Lu *et al.* 2015, Weng *et al.* 2015, Fan *et al.* 2016). Bakhtar *et al.* (1997), Li *et al.* (2002), and Li *et al.* (2013) used physical model tests to study blasting loads, seepage in rock fractures, stress-strain responses and stability during inland and offshore tunneling. Bae *et al.* (2007) studied the deformation of segmental retaining walls by a series of scale-down models. Ding *et al.* (2011) used a three-dimensional (3D) geomechanical model to investigate the progressive failure as well as the failure modes of a concrete gravity dam if the foundation rock was treated and untreated. More recently, through model tests, Miller and Gustin (2013) came up with measures to prevent and control the non-point source mercury leakage from the OP gold mine. In summary, the model test has made it possible to scale down a problem and experimentally study it by at least preserving the key parameters of interest.

Yanqianshan Iron Mine, located in Liaoning Province, is a major ore deposit of Northern China, which had been in operation for years and was in the transition from merely OP mining to OP and UG joint mining to maintain its productivity. Previously, based on the so-called “Equivalent Jointed Rock-mass Model (EJRM)”, Xu *et al.* (2016)

analyzed the stability of rock mass of the mine, and investigated complex mechanical behaviors of rock masses induced by UG mining in the iron ore. According to the calculated results, the displacement and degree of destruction of surrounding rocks in the mining area were mainly governed by the overburden stress of rocks and the characteristics of the joints and their distribution. It also concluded that the movement and crashing of surrounding rocks of the mining area made the slope surface subside downward and slide inward to the pit. However, due to the limitation of numerical calculation, it was difficult to illustrate the progressive movement and failure process caused by transition from OP to UG. To reveal the dynamic process of deformation and movement of the slope during the transition from OP to UG mining, this study selected the Yanqianshan Iron Mine as the prototype and, afterward, built and tested a large-scale 2D model according to the similar theory. The model was instrumented by 3D laser scanning technology, distributed fiber strain monitoring technology, and digital photogrammetry to monitor the deformation and strain of the OP slope throughout the test. The yielded data provided information for the prediction of slope movement and failure, which could be used to identify remedial measures to control the excessive deformation and movement of the OP slopes in the future. Moreover, a numerical simulation was adopted to further reveal the details of the deformation and failure mechanism of pit slope, which could not be easily seen in the model test.

2. Model test design

2.1 Engineering geology condition of mining area

One After decades of OP mining, a large pit in

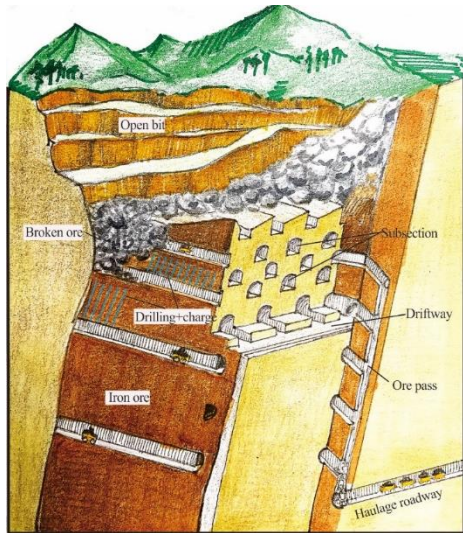


Fig. 2 Non-pillar sublevel caving method (modified from Brady and Brown 2006)

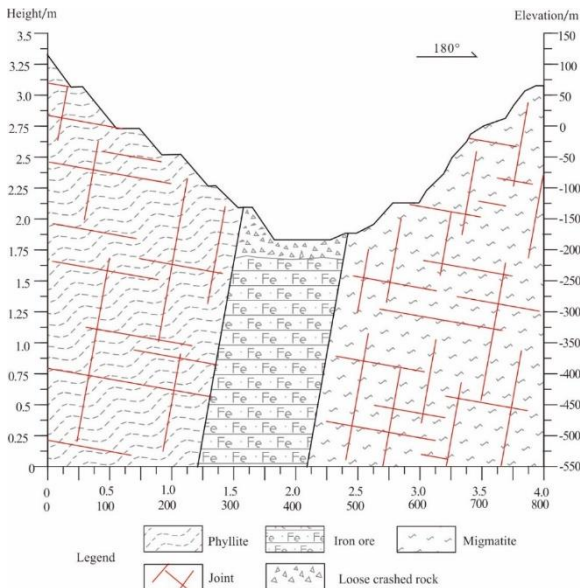


Fig. 3 Geological section of the A-A' section

Yanqianshan Iron Mine has formed, which is 1,410 m long from east to west, 570-710 m wide from south to north, and about 250 m deep, as shown in Fig.1. The overall inclination angle of the pit slope is about 40°. The mining area as hatched in green in the topography shown in Fig.1 extends roughly along the east-west direction; consequently, mining activities are mainly constraint in this green strap area. The field visit reported different local failures, including collapse, landslide, and tension cracking, on the east and west sides of the pit, caused by iron ore mining disturbance as marked in Fig. 1.

Long-term mining activities, including digging, blasting, crashing and hauling, have created numerous fractures in the rock mass that may be temporarily stable due to friction and interlocking between rocks. The frequent vibration generated by routine mining activities facilitates progressive movement of such rocks towards the pit, which may trigger sudden collapses or landslides. In addition, the creeping

Table 1 Similarity ratios of different parameter according to the dimensional method (Zou *et al.* 2013)

Symbols	Notations	Formula
C_σ	Normal stress similarity ratio	$C_\sigma = C_r C_L$
C_τ	Shear stress similarity ratio	$C_\tau = C_\sigma$
C_E	Elastic modulus similarity ratio	$C_E = \frac{C_\sigma}{C_\varepsilon}$
C_μ	Poisson's ratio similarity ratio	$C_\mu = 1$
C_ε	Strain similarity ratio	$C_\varepsilon = 1$
C_ϕ	Friction angle similarity ratio	$C_\phi = 1$

Table 2 Physical and mechanical properties of migmatite and phyllite and their similar materials

Rock type	Density (kg/m ³)	Unconfined compressive strength (MPa)	Elastic modulus (MPa)	Cohesion (MPa)	Internal friction angle (°)
Migmatite and phyllite	2500	140~300	3000~5000	40~50	38~40
Similar material	2500	0.7~1.5	150~250	0.2~0.25	38~40

Table 3 Physical mechanical parameters of similar materials

Name	Density (g/cm ³)	Uniaxial compressive strength (MPa)	Elastic modulus (MPa)	Cohesion (MPa)	Internal friction angle (°)
Target value	2.5	0.7~1.5	150~200	0.2~0.25	38~40
Achieved value	2.56	0.80	200.6	0.17	38.94

movement of the lower rocks may result in the formation of tension cracks in upper rocks, which may collapse or roll over later on. The field investigation to the mine also disclosed that on the east side of the pit the failure planes were primarily coincident with the structural plane of the rock formation, shown in Fig. 1(d). In addition, the tension cracks were salient in many locations, especially at the scarps of the slides as shown in Fig. 1(b). In contrast, the slope on the west side was gentler than that on the east side; as a result, progressive landslide and large area subsidence were more common than other types of distress modes as shown in Fig. 1(a) and 1(c).

In general, the failures were primarily localized and there was no foreseen risk of global failure at the time of the field visit. However, to maintain the productivity, the mining had to be transitioned to UG with a non-pillar sublevel caving method as shown in Fig. 2, which can significantly influence the stability of the OP slopes, especially at the location of the main entrance of the UG mining.

In this paper, the A-A' Section as marked in Fig. 1 was used as the prototype slope of the model test to assess the induced movement. This location was selected as the main entrance of the vertical shaft mining because it potentially had a minimal impact on the surrounding slopes. At this cross-section, the slopes in north-south direction had a run of approximately 800 m and a rise of approximately 650 m. The south and north slopes were the results of years of mining. The south slope was mainly composed of migmatite, while the north slope was mainly phyllite. Both

slopes had a height of approximately 250 m, sloping at an angle roughly 40°. The elevations of their toes were about -183 m and their crest elevations were about 70 m. The bottom of the OP, ranging from -183 m to -215 m, consisted of a loose rock layer and then an underlying competent rock layer. The loose rock layer was the result of enduring mining activities for many years, which was significantly fractured, forming a loose crashed rock cushion. The underlying competent layer was formed due to the intrusion of rock into the ore deposit in geological age. The iron ore deposit resumes from an elevation of -215 m ~ -500 m, which would be the future UG mining space.

As mentioned previously, the non-pillar sublevel caving method would be adopted for the UG mining with the height of each segment to be 18 m. For the purpose of this experimental study, the prototype slope and its scale-down model are both shown in Fig. 3. The right vertical axis of the figure shows the true elevation, while the left vertical axis shows the dimensions used in model test, which were determined based on the similar theory. The true and model dimensions in the horizontal direction are both shown in the horizontal axis. The regional geological data shows that the surface rock of the mining is part of the rock strata that inclined at an angle of 70°, extending North-East. The rock mass mainly contains two sets of dominant joints, which dip at an angle of 10° and 80°, respectively, as marked in red in Fig. 3.

2.2 The ratio of similar materials

Considering containable dimension in the lab, the geometric similarity ratio was selected to be 200, namely, $C_L=200$, which is illustrated in Fig. 3. The similarity ratio of density was selected as 1, i.e., $C_r=1$ based on comparison and analysis of many sets of similarity scales. The similarity ratios of other parameters were derived from the selected C_r and C_L according to the similarity theory as shown in Table 1.

Stress similarity parameter

$$C_\sigma = C_\tau = C_E = 200 \quad (1)$$

where C_σ , C_τ and C_E are the similarity ratio of stress, shear strength, and elastic modulus, respectively. Poisson's ratio, strain, internal friction angle similar parameters

$$C_\mu = C_\varepsilon = C_\phi = 1 \quad (2)$$

where C_μ , C_ε and C_ϕ are the similarity ratio of Poisson's ratio, strain, and internal friction angle, respectively.



Fig. 4 Cylindrical specimens

Migmatite and phyllite rock samples had been retrieved from the site, and cored specimens were tested for their properties in the lab as a part of the design tasks of the UG mining. Table 2 shows the physical and mechanical properties of the rocks as well as the expected properties of their similar materials, which were calculated based on the similarity ratios listed in Table 1.

Cement, quartz sand, barite powder, iron ore powder and gypsum were selected as ingredients to prepare for the similar materials that would be used for the model test. To achieve the target properties listed in Table 2, the ingredients were mixed by 30 different ratio combinations. For each ratio combination, ten cylindrical specimens with a diameter of 50 mm and height of 100 mm (shown in Fig. 4) were casted, cured and tested for their density, compressive strength, elastic modulus, internal friction angle, and cohesion. It was found that a weight ratio of 1 : 28 : 28 : 6.67 : 3 : 2 (i.e., cement : quartz sand : barite powder : iron ore powder : gypsum : water) led to the desired properties as shown in Table 3. The mixture was mixed by manual agitation (clockwise stirring and counterclockwise stirring) and cured at room temperature of 20 ± 2 °C and humidity of $60 \pm 10\%$. Thus, this combination was used to prepare for the ore materials used in this study.

2.3 Test system

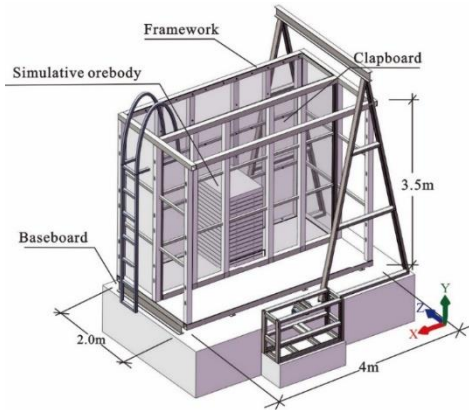
2.3.1 Model chamber

The model test was performed in a test chamber as shown in Fig. 5, which had a dimension of length 4,000 mm × width 1,000 mm × height 3,500 mm. The test system was made of four parts: baseboard, framework, clapboard, and simulative orebody. To facilitate observation during the test, the three sides of chamber were made of transparent polycarbonate (PC) board and braced by steel beams, which was tested in advance to ensure that they would not deform excessively during testing. The backside of the chamber was constraint by a 10 mm thick steel plate. It should be mentioned that the clapboard in the middle of framework was movable to accommodate different dimension in Z-direction as marked in Fig. 5(a); thus, a 2D or 3D model test can be conducted in this chamber.

2.3.2 Deep mining simulation system

According to the similarity theory, the north-south width of the simulation orebody (i.e., the UG mining zone) is 800 mm (X-direction of the model is shown in Fig. 5(a); the cross-section is shown in Fig. 3), the east-west distance is 1,000 mm (Z-direction) and the mining depth is 1,425 mm (Y-direction) under the condition of geometric similarity ratio of 200.

Based on the characteristics of the non-pillar UG mining method, the whole mine model was divided into three zones: north slope, south slope and UG excavation area. The blocks of the similar material with a dimension of 150 mm × 150 mm × 150 mm were used to reconstruct the north and south slopes as shown in Fig. 5(b). Such a dimension was selected so the dominant fracture could be well represented. The blocks were placed in an inclined angle so that the sides of each block were oriented in the direction



(a) Schematics



(b) Test in progress

Fig. 5 Illustration of the test chamber

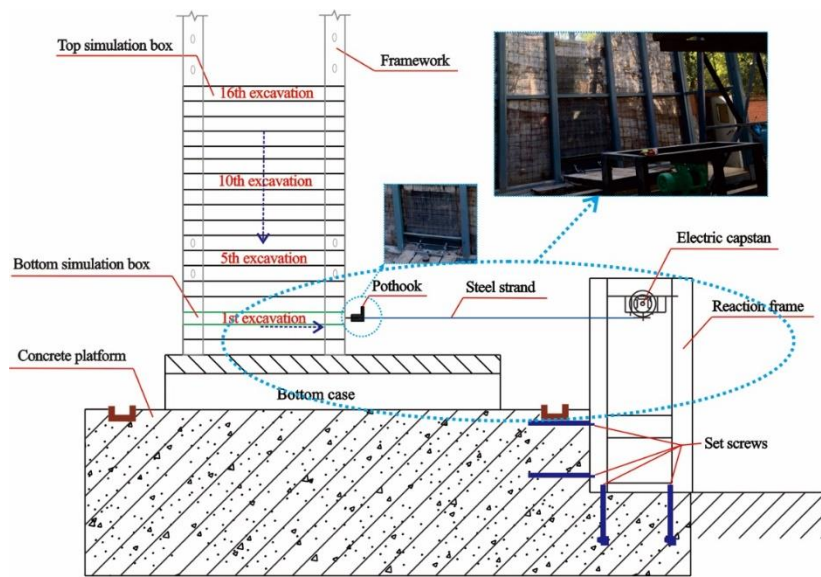


Fig. 6 Schematics of the test chamber, transmission system and test setup

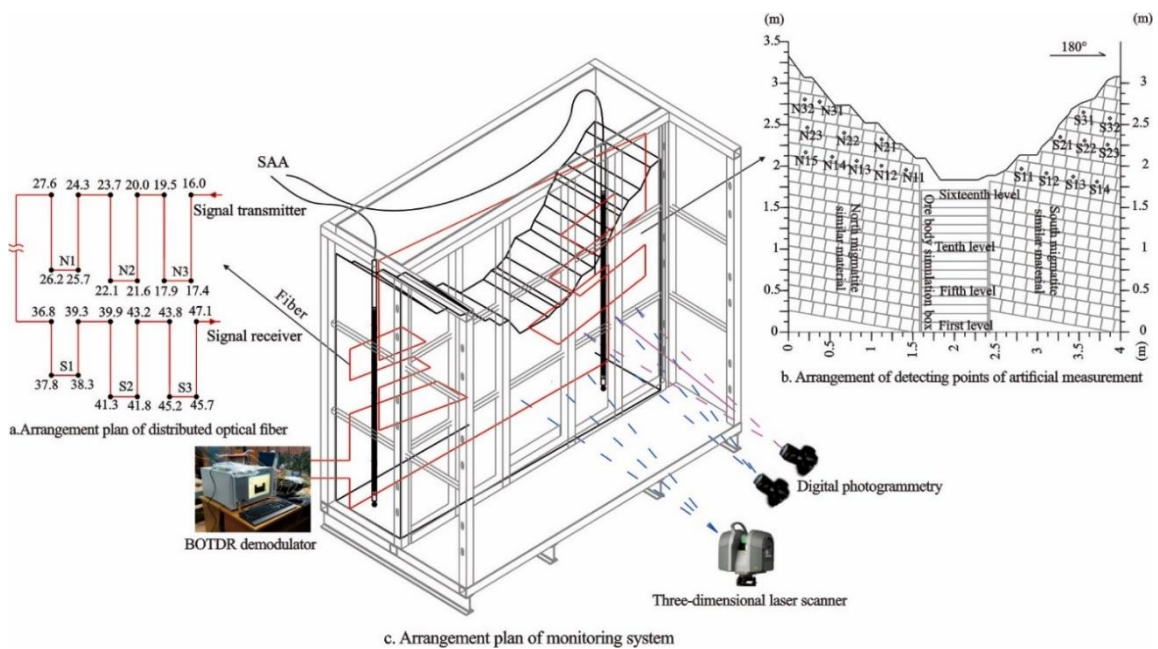
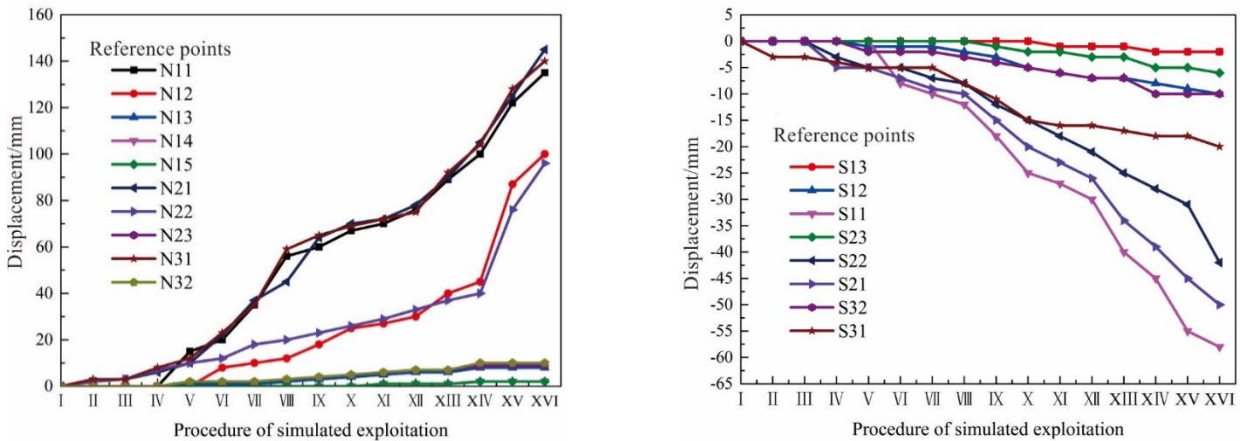


Fig. 7 Schematics of monitoring system layout (N - north; S - south)



Fig. 8 Schematic diagram of the simulation of excavation



(a) Curves of north migmatite displacement of detecting points (b) Curves of south migmatite displacement of detecting points

Fig. 9 Horizontal displacement curves of the north and south end slopes

of the dominant joints on the both slopes as indicated in Fig. 3 as the joints were vital to failure of rock structure (e.g., Shemirani *et al.* 2017). In contrast, the excavation area was constructed with 16 layers of simulation boxes made of pre-casted slabs and the dimension of each box is 995 mm × 800 mm × 90 mm (length × width × height). The height of simulation box was selected according to the real UG mining sublevel. The depth of underground mines ranged from Elevation -215 to Elevation -500 m, which was anticipated to consist 16 sublevels of mining: 15 sublevels that each has a height of 18 m, and one bottom sublevel with a height of 15 m. According to a similarity ratio of 200, each sublevel of UG mining was represented by a

height of 90 mm in the test model. Even though the bottom sublevel should be 75 mm, it was represented by 90 mm to simplify the simulation boxes preparation. This slight discrepancy was not expected to introduce significant error into the results. It is noteworthy that each slab was framed in steel wires before being put in the test chamber, which made the simulation of the excavation possible. In this test, all the blocks interacted with each other through friction and interlock and no artificial cementation was created.

To facilitate the model test, a loading and reaction system was built to remove orebody, piece by piece, to simulate excavation; and apply additional loads if needed,

which is schematically shown in Fig.6. The simulation of each sublevel of excavation was executed in the following procedure: firstly, the electric capstan and steel strand were connected with the bottom simulation box by the high strength threaded buckles; secondly, the box was pulled out to create a cavern in ore body, similar to the non-pillar sublevel caving mining method. The above steps were repeated until the simulated excavation was completed. The procedure is illustrated in Fig. 6.

2.3.3 Monitoring system design

The test model was monitored by distributed optical fibers, which were buried during model construction (Fig. 7(a)), 3D laser scanner and digital photogrammetry (Fig. 7(b) and (c)) and Shape Accel Array (SAA) inclinometer (Fig.7(c)). No contacting methods, i.e., 3D laser scanner and digital photogrammetry, were used to capture the slope surface movement caused by the excavation, while distributed optical fibers and SAA inclinometer were used to monitor the distribution of the strain and movement, respectively, within the mass. A few selected reference points on the north and south slopes were marked to provide targets for the photogrammetry as shown in Fig. 7(b). The monitoring system integrated the contact and non-contact methods, which could yield comprehensive data on the movement and deformation of the testing model.

3. Test results and analysis

The model test was carried out in stages according to the approach described previously. After each excavation (i.e., removing each simulation box), the data from all instruments were collected a few times before advancing to the next stage to ensure an equilibrium was reached. Unfortunately, due to the damage of the SAA inclinometer, its monitoring data were not available.

3.1 The data from digital photogrammetry

The crack development at different stages of mining is shown by photos in Fig. 8, and the horizontal displacement curves of north and south slopes are shown in Fig. 9, in which displacements toward south are defined as positive, vice versa (refer to Fig. 7(b) for the location of north and south slopes).

It can be seen from Fig. 9 that all the reference points of both south and north slopes moved towards the mined-out area, that is, the horizontal displacements increased with the increase of the UG mining depth. The rock closer to the mined-out area moved more than other areas. Overall, the horizontal displacement of south slope was obviously smaller than the north one. After the completion of the excavation, the maximum horizontal displacement of the south slope was only 58 mm, while that of the north slope reached 145 mm. This phenomenon is mainly because the north slope was the bedding slope, in which the principal joints leaned towards the mine-out area as shown in Fig. 7(b). Such orientation of the joints facilitated the downward sliding movement of rocks. As a result, the horizontal displacement was larger, and the influence range was wider.

However, the south slope had a reversed slope, in which the joints were oriented against the mine-out area as shown in Fig. 7(b). Different from the north slope, such orientation of joints provided interlocks between rocks; thus, the horizontal displacement and the influence range were smaller.

3.2 The data from 3D laser scanning

Based on the 3D laser scanning, the point clouds of the whole model at different stages of excavation were obtained. The crack generation and propagation were analyzed by Geomagic qualify software. The following sequence was applied to ensure the results were comparable. Firstly, the model was scanned before the excavation to restore the initial positions. The point clouds obtained by scanning were colored and cut, and then non-connected items and external solitary points were removed to reduce noise. Thereafter, the point clouds were encapsulated and transformed into polygon model that can be used as the reference object for subsequent excavation. Then, the same procedure was repeated for each excavation. At last, 3D deviation calculation of the reference and test objects was carried out in the software platform to obtain the information of the crack initiation and propagation, which are shown in Fig. 10.

According to Fig.10, it can be found that three fractures (delineated in red ellipse) appear at the north slope after the completion of the 4th step of the excavation, which were nearly vertical and approximately in the direction of rock joints. The extension of the fracture gradually decreased with regards to its distance from the toe of the slope. But at this stage no obvious crack was observed on the south slope, which was basically consistent with the measurement of the displacements. At the 8th step of excavation, the fractures of the north slope significantly deepened; at the meantime, some shallow fractures appeared on the south slope. At the 12th step of the excavation, numerous cracks became obvious on the south slope and collapse occurred on the north slope (Fig. 10(c)). After the completion of the excavation, collapse was also observed on the south slope. (Fig. 10(d)). In general, the depth and width of the fracture at the north slope were larger than those at the south slope.

3.3 The data from distributed optical fibers

The optical fiber was mainly used to monitor the strain within the mass during the model test. The optical fiber arrangement is shown in Fig. 7(a) and 7(c). The monitoring results are shown in Fig. 11, in which the tensile strain is positive, and the compressive strain is negative. At the 10th stage of excavation, the fiber optic was pulled out; as a result, the fiber optic data collection was terminated at this step.

It can be concluded from the distribution of strain along the optical fiber of the north slope that the internal strain of the model increased with the excavation. The strain at most of the locations were trivial except for three spikes, which represented strains at the fiber length of 17.7 m, 21.4 m and 26.6 m, respectively. The location and strains are plotted in Fig. 12. By comparing Figs. 10 and 12, it appears that these

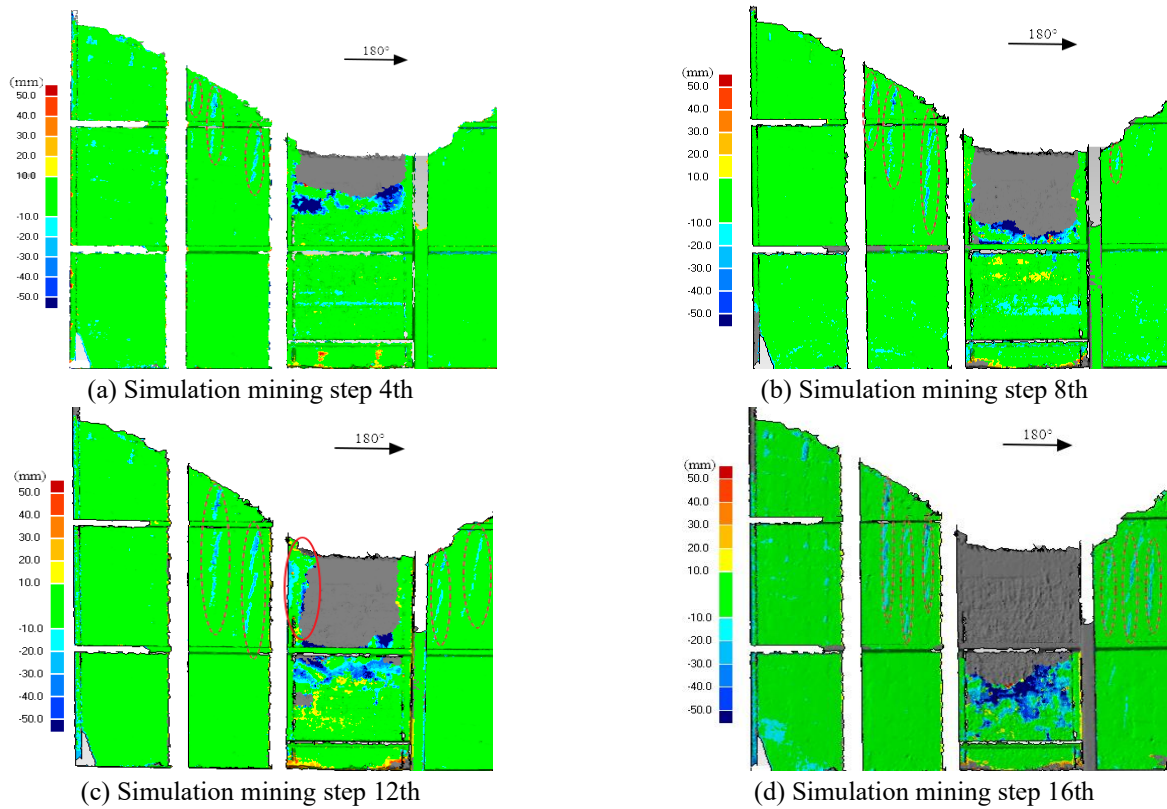


Fig. 10 Comparison of three-dimensional point clouds after each simulated mining step

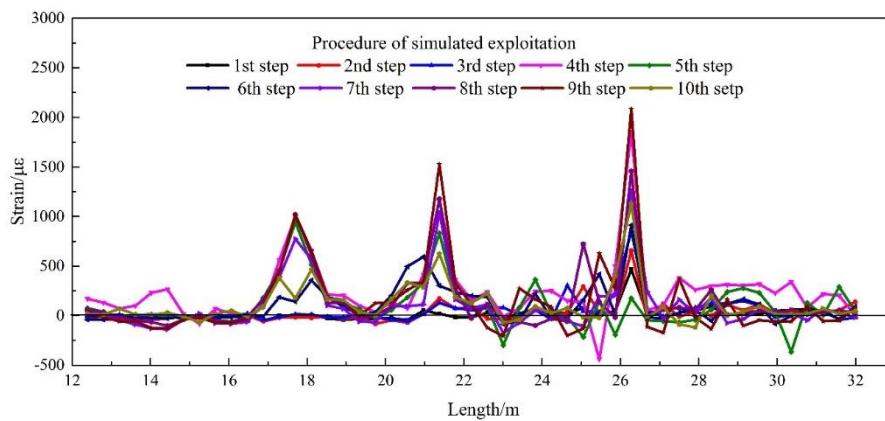


Fig. 11 Optical fiber strain curve

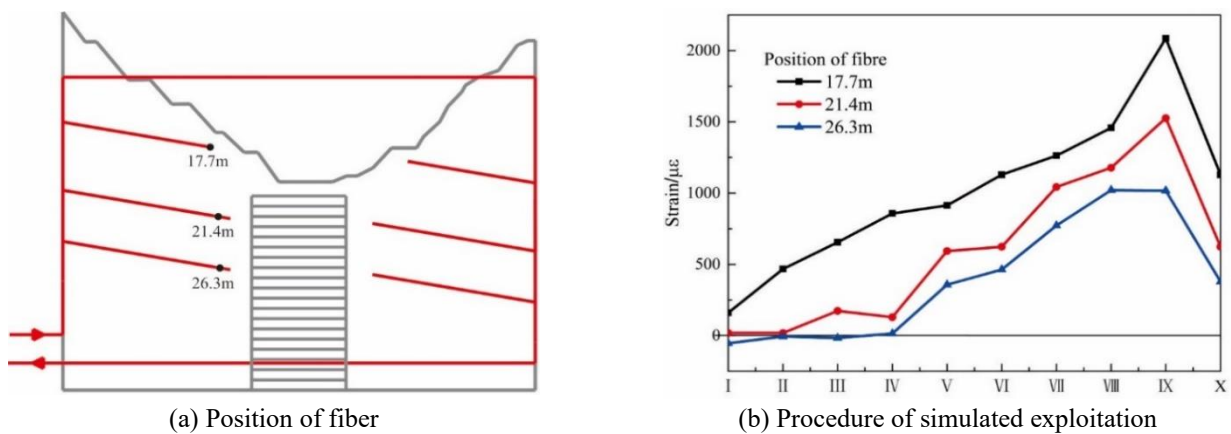


Fig. 12 Optical fiber distribution and strain curves at different locations of northern slope

Table 4 Mechanical parameters of the structural plane

Serial number	Zones	Internal friction angle ϕ (°)	Cohesion c (MPa)	Normal stiffness k_n (GPa)	Shear stiffness k_s (GPa)
1	North slope	16.85	0.34	5.06	1.91
2	Ore body	19.14	0.56	5.92	2.22
3	South slope	26.42	1.02	7.32	3.52

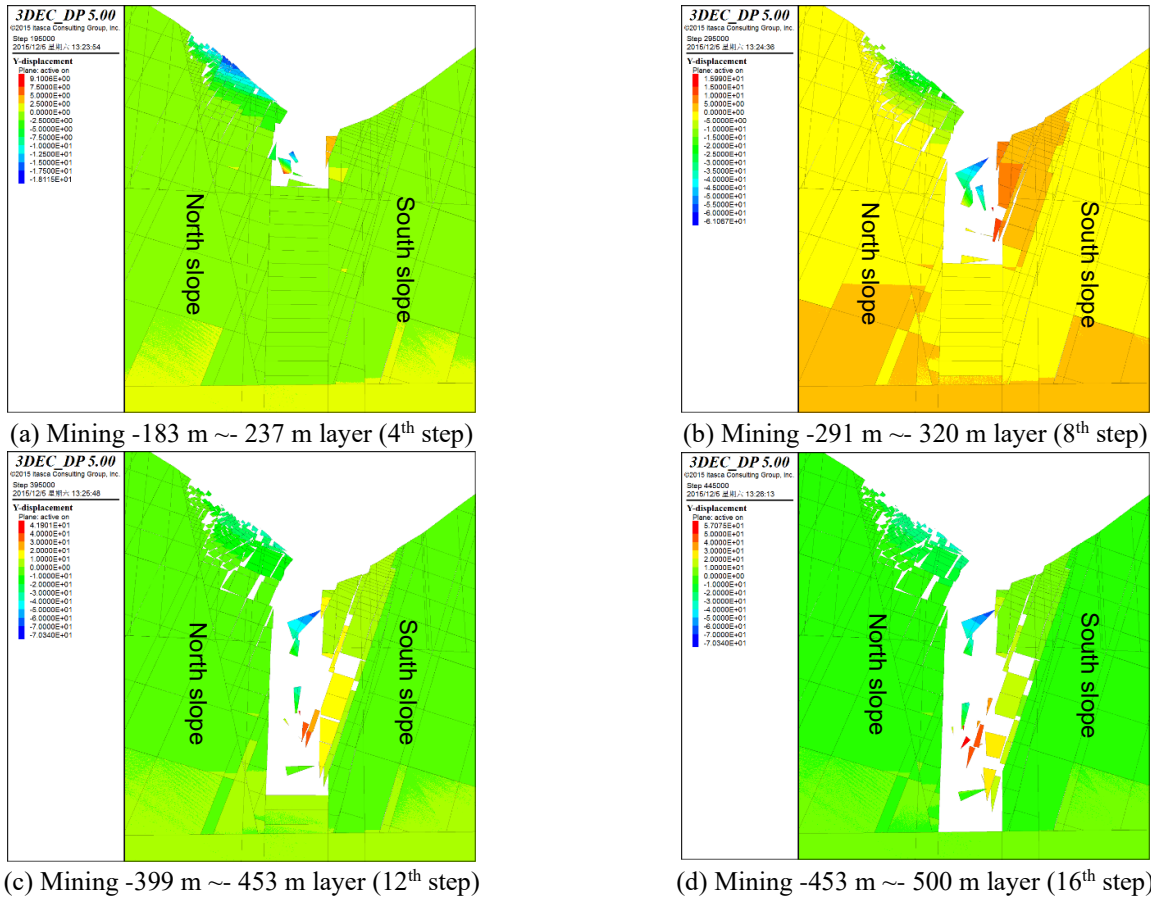


Fig. 13 Deformation contour of numerical simulation at different stages of excavation

three points were coincidentally located very close to one of the major cracks. At the same time, it can be found out in Fig. 12(b) that when the 10th step excavation was completed, the strain started to drop, which was attributed to the slip between the optical fiber and the burying material, leading to disengagement between the optical fiber and the materials. At the position located 17.7 m of the optical fiber, namely, the toe of the north slope, the strain was detectable since the first step excavation, and the strain was gradually increased with the excavation, which reached its maximum value of 2,085 $\mu\epsilon$ at the 9th step of excavation. At the position located 21.4 m of the optical fiber, significant strain began to appear at the 3rd step of excavation, and the maximum value was 1,525 $\mu\epsilon$ at the end of the 9th step of the excavation. At the position located 26.3 m of the optical fiber, significant strain began to appear at the end of the 5th step of excavation, and the maximum value of 1018 $\mu\epsilon$ was reached at 9th step of excavation. It is worth mentioning that at the 5th step, the excavation has not reached the depth where the 26.3 m fiber was located. However, due to the movement of the surrounding rock, the

strain about 357 $\mu\epsilon$ was detected at that location. This strain information appears to suggest the cracking likely start from lower elevation.

4. Numerical calculation

Upon the completion of the model test, a full-scale numerical simulation was conducted using the discrete element numerical simulation software - 3DEC to further validate the findings from the model test in a full-scale setting. The discrete element method was selected over constitutive modeling such as Gu *et al.* (2018) because it can better manifest the cracking process. The dimension of numerical model was 5,000 m (length) \times 3,400 m (width) \times 800 m (height), which made the size of this model at least 3 times of the real mining area to eliminate the boundary effect. The model contained 1,421,500 grid points and 189,827 blocks. And the minimum size of block is 25 ~ 20 m. The left and right boundaries of the model were constraint from horizontal displacements, and the bottom

boundary was fixed for vertical displacements. The horizontal deformation contour is shown in Fig. 13.

There were a large number of primary and tectonic joints in this area (Xu *et al.* 2016), which would potentially influence the deformation and failure of surrounding rocks. Therefore, these joints must be appropriately accounted in the numerical model. To make the computing time reasonable without omitting the most important features of the rock mass in the simulation, the following simplifications were adopted:

- Only the main joints in the mining area were considered, and the secondary joints were neglected;
- The same group of joints were represented by parallel interface planes, and the trend and dip of joints was determined according to the average of the same group; and
- In the area close to mining excavation, the joints were densely spaced, while in other areas the joints were relatively sparse.

The rock was assumed rigid and the interaction of rocks at the joints were simulated by frictional interfaces, which were characterized by normal stiffness k_n , shear stiffness k_s , cohesion c and internal friction angle ϕ , as listed in Table 4 (Xu *et al.* 2016; Lian *et al.* 2015).

Fig. 13 is the displacement contours obtained from the numerical simulation, which indicates that the north and south slopes behaved noticeably different. As to the north slope, the mining mainly triggered sliding and rotation towards the mined-out area due to the removal of the support at the toe of the slope. This is largely attributable to the orientation of the rock joints, which facilitates the downward creeping. Since the formation of rocks leaned downward, the rotational movement is also pronounced upon the removal of the support at the toe. When the excavation proceeded deeper and deeper, separation between layered rock became salient and rock was subjected to considerable bending, which eventually caused rupture. Even though the south slope was not as steep or high as the north slope, it started to fail locally at an earlier stage. It should be noted that the discrete element numerical simulation software - 3DEC treats materials as numerous discrete elements that interact with each other through contacts, which cannot provide the factor of safety of slope from a limit equilibrium analysis.

5. Discussion of the results

Before the transition from OP to UG mining, the mining pit slopes overall were stable, except for a few localized collapses. With initiation and propagation of UG mining, rock mass started to show noticeable global movement on both north and south slopes. The model test and numerical analysis both disclosed that the global movement and failure induced by transition from OP to UG mining could be roughly categorized into three stages. From the 1st to the 4th step of excavation, the movements of the south slope were rather limited. Even though both model test and numerical simulation detected some emerging minor crack in the rock mass of the north slope, it remained largely stable. From the 5th to the 12th step of the excavation, the UG mining was extended to a great depth, the movements

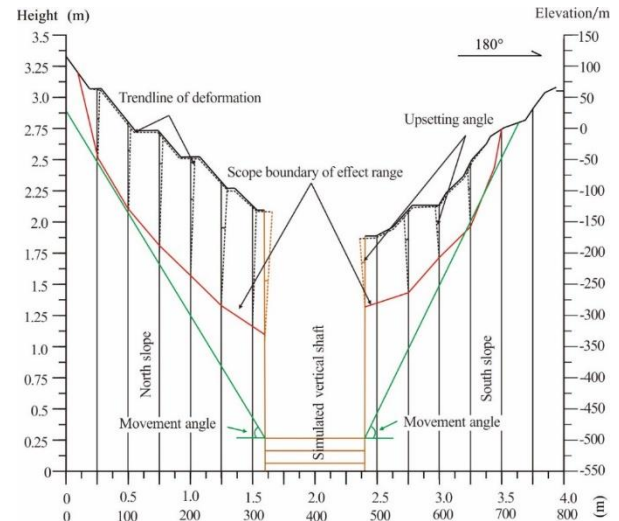


Fig. 14 Schematics of the deformation trend of the model

of both slopes increased rapidly. The separation between rock layers and tension crack in rock became salient on the north slope and, at the same time, the slope started to fail along the planes of major joints with noticeable amount of cave-in to the mine-out area. The increase of internal strains at this stage was also enormous as the optical fiber embedded in the slope was pulled out during the model test, implying the accumulated strains were excessive. From the 12th step and thereafter, various regional collapses in the south slope occurred, while the north slope had massively failed.

Based on the model test and numerical simulation, it could be concluded that the failure mode of the slope was predominantly controlled by the structural fractures that included joints and bedding surfaces. In this work, the rotation angle (upsetting angle) is defined as the vertical angle before and after rock movement (Fig. 14). To measure the rotation angle, each slope was divided into 7 vertical slices as shown in Fig. 14 and the rotation at the vertical boundary between adjacent slices were quantified from the numerical results. Movement angle is defined as the intersection between sliding surface the horizontal line (Fig. 14). The sliding surface was obtained from the shear strain rate contours. The rotation angle of the north slope was between $4.3^\circ \sim 8.2^\circ$, and the movement angle is about 60° ; the rotation angle of the south slope was between $0.6^\circ \sim 3.9^\circ$, and the movement angle is about 70° (Fig. 14). The damage of rock was primarily attributable to the existence, development and extension of the fractures in the rock mass. A cracking zone could be delineated by connecting the tip points of each crack on the north and south slopes, respectively, which is shown in red lines in Fig. 14. The zones on the slopes were approximately circular, but the north slope obviously had much larger influential range.

6. Conclusions

This paper is based on a combined experimental and numerical study of Yanqianshan Iron Mine, which was in the transition stage from OP to UG mining. A large-scale model test and a full-scale numerical analysis were used to

assess the stability of rock slope and movement of rock mass during the transition period. Based on the results of the model test and numerical simulation, the following conclusions can be drawn:

- Underground mining during transition from OP to UG mining is a major trigger of the pit slope movement, especially for rock slope with existing fractures from prior mining activities. The distress modes of the rock primarily included tension crack, sliding, overturning and collapse, which depended heavily on the orientation of the joints. If the rock joints were more or less in alignment with the slope surface, i.e., the different between dip angle of the rock joints and inclination angle of the slope was small, sliding was more likely to dominate. In contrast, if the dip angle differed from the inclination angle of the slope significantly, overturning may become the major failure modes. For both sliding and overturning, tension crack could develop extensively, causing separation between adjacent rocks. Such separation could lead to rock falls at the toe of the sliding mass and at the crown of the overturning mass.

- The technologies used in this study to monitor the movement or strain of the rock mass achieved satisfactory results, showing their advantages over conventionally used instrumentations. Distributed optical fiber technology can be used to monitor the strain in testing models, which has the advantages of high precision and strong anti-interference ability and, more importantly, if planned well, it can provide location and strain information at the same time. 3D laser scanning technology can be used to observe the surface deformation of a large model with the assistance of point clouds approach, which is especially suitable for large areas or areas of limited accessibility. The digital photogrammetry technique can be used to observe the displacement of reference points.

- The model test of a miniature of real world situation would be representative if the similar theory is used to control the dimension and properties of the materials. Dimension analysis can be used to determine the appropriate properties considering the allowable size in the lab.

However, it is noteworthy that the model test of this paper was two-dimensional and may not be able to account for the impact of the orientation of the strike of the rock formation. Thus, a three-dimensional study may be able to provide more information.

Acknowledgments

This work is funded by the National Natural Science Foundation of China (Nos. 61427802, 41572301, 51778217, and 41972030) and the Fundamental Research Funds for the Central Universities of China (No. 2652018108). Additionally, the authors would like to acknowledge the editors and anonymous reviewers for their valuable comments and suggestions, which significantly improve the quality of this paper.

References

Bae, W. and Woo, K.J. (2007), "A study on the deformation

- behavior of the segmental grid retaining wall using scaled model tests", *Tunn. Undergr. Sp. Technol.*, **17**(5), 350-359.
- Bakhtar, K. (1997), "Impact of joints and discontinuities on the blast-response of responding tunnels studied under physical modeling at 1-g", *Int. J. Rock Mech. Min. Sci.*, **34**(3-4), 1-15. [https://doi.org/10.1016/S1365-1609\(97\)00143-3](https://doi.org/10.1016/S1365-1609(97)00143-3).
- Bakhtavar, E, Shahriar, K. and Orace, K. (2009), "Transition from open-pit to underground as a new optimization challenge in mining engineering", *J. Min. Sci.*, **45**(5), 485-494. <https://doi.org/10.1007/s10913-009-0060-3>.
- Bakhtavar, E. (2013), "Transition from open-pit to underground in the case of Chah-Gaz Iron Ore combined mining", *J. Min. Sci.*, **49**(6), 955-966. <https://doi.org/10.1134/S1062739149060166>.
- Brady, B.H.G. and Brown, E.T. (2006), *Rock Mechanics for Underground Mining*, Springer.
- Bye, A.R. and Bell, F.G. (2001), "Stability assessment and slope design at Sandsloot open pit, South Africa", *Int. J. Rock Mech. Min. Sci.*, **38**, 449-466. [https://doi.org/10.1016/S1365-1609\(01\)00014-4](https://doi.org/10.1016/S1365-1609(01)00014-4).
- Chung J., Topal, E. and Ghosh, A. K. (2016), "Where to make the transition from open-pit to underground? using integer programming", *J. S. Afr. Inst. Min. Metall.*, **116**(8), 801-808. <https://doi.org/10.17159/2411-9717/2016/v116n8a13>.
- Ding, Z.L., Zhang, L., Chen, Y. and Hu, C.Q. (2011), "3D geomechanical model failure test on stability against deep sliding of gravity dam", *J. Hydraul. Eng.*, **42**(4), 499-504 (in Chinese). <https://doi.org/10.13243/j.cnki.slxb.2011.04.015>.
- Fan, Z.J., Kulatilake, P.H.S.W., Peng, J.B., Che, W.Y., Li, Y.Z. and Meng, Z.J. (2016), "In-flight excavation of a loess slope in a centrifuge model test", *Geotech. Geol. Eng.*, **34**, 1577-1591. <https://doi.org/10.1007/s10706-016-0067-x>.
- Fumagalli, I.E. (1973a), *Linearly-Elastic Static Models*, Springer Vienna, Austria, 58-83.
- Fumagalli, I.E. (1973b), *Model Simulation of Reinforced and Prestressed Concrete Structures*, Springer, Vienna, Austria, 84-117.
- Fumagalli, I.E. (1973c), *Physico-Mechanical Properties to be reproduced in the Model Materials*, Springer, Vienna, Austria, 14-32.
- Gu, J.C., Gu, L.Y., Chen, A.M., Xu, J. and Chen, W. (2008), "Model test study on mechanism of layered fracture within surrounding rock of tunnels in deep stratum", *Chin. J. Rock Mech. Eng.*, **27**(3), 433-438 (in Chinese). <https://doi.org/10.3321/j.issn:1000-6915.2008.03.001>.
- Gu, Q., Ning, J., Tan, Y., Liu, X., Ma, Q. and Xu, Q. (2018), "Damage constitutive model of brittle rock considering the compaction of crack", *Geomech. Eng.*, **15**(5), 1081-1089. <https://doi.org/10.12989/gae.2018.15.5.1081>.
- He, M.C., Feng, J.L. and Sun, X.M. (2008), "Stability evaluation and optimal excavated design of rock slope at Antaibao open pit coal mine, China", *Int. J. Rock Mech. Min. Sci.*, **45**, 289-302. <https://doi.org/10.1016/j.ijrmm.2007.05.007>.
- Korkmaz, H., Cetin, B., Ege, I., Karatas, A., Bom, A. and Ozsahin E. (2011), "Environmental effects of stone pits in Hatay (Turkey)", *Procedia Soc. Behav. Sci.*, **19**, 504-510. <https://doi.org/10.1016/j.sbspro.2011.05.162>.
- Li, S.C., Song, S., Li, L., Zhang, Q. and Wang, K. (2013), "Development on subsea tunnel model test system for solid-fluid coupling and its application", *Chin. J. Rock Mech. Eng.*, **32**(5), 883-890 (in Chinese). <https://doi.org/10.3969/j.issn.1000-6915.2013.05.005>.
- Li, Z.K., Xu, Q.J., Luo, G.F. and Wang, A.M. (2002), "Three dimensional geomechanical model test of large underground hydropower station group", *J. Hydraul. Eng.*, **31**(05), 31-36 (in Chinese). <https://doi.org/10.3321/j.issn:0559-9350.2002.05.007>.
- Lin, P., Liu, X.L., Zhou, W.Y., Wang, R.K. and Wang, S.Y. (2015), "Cracking, stability and slope reinforcement analysis relating to

- the Jinping dam based on a geomechanical model test”, *Arab. J. Geosci.*, **8**(7), 4393-4410. <https://doi.org/10.1007/s12517-014-1529-1>.
- Lu, P., Wu, H.B., Qiao, G. and Li, W.Y. (2015), “Model test study on monitoring dynamic process of slope failure through spatial sensor network”, *Environ. Earth Sci.*, **74**(4), 3315-3332. <https://doi.org/10.1007/s12665-015-4369-8>.
- Miller, M.B. and Gustin, M.S. (2013), “Testing and modeling the influence of reclamation and control methods for reducing nonpoint mercury emissions associated with industrial open pit gold mines”, *J. Air Waste Manage. Assoc.*, **63**(6), 681-693. <https://doi.org/10.1080/10962247.2013.778221>.
- Nguyen, P.M.V.N. and Niedbalski, Z. (2016), “Numerical modeling of open pit (OP) to underground (UG) transition in coal mining”, *Stud. Geotech. Mech.*, **38**(3), 35-48. <https://doi.org/10.1515/sgem-2016-0023>.
- Ordin, A.A. and Vasil’ev, I.V. (2014), “Optimized depth of transition from open pit to underground coal mining”, *J. Min. Sci.*, **50**(4), 696-706. <https://doi.org/10.1134/S1062739114040103>.
- Rose, N.D. and Hungr, O. (2007), “Forecasting potential rock slope failure in open pit mines using the inverse-velocity method”, *Int. J. Rock Mech. Min. Sci.*, **44**, 308-320. <https://doi.org/10.1016/j.ijrmms.2006.07.014>.
- Shemirani, A. B., Haeri, H., Sarfarazi, V. and Hedayat, A. (2017), “A review paper about experimental investigations on failure behaviour of non-persistent joint”, *Geomech. Eng.*, **13**(4), 535-570. <https://doi.org/10.12989/gae.2017.13.4.535>.
- Song, J.Y. and Choi, Y. (2016), “Analysis of the potential for use of floating photovoltaic systems on mine pit lakes: case study at the Sangyong open-pit limestone mine in Korea”, *Energies*, **9**(2), 102. <https://doi.org/10.3390/en9020102>.
- Wang, L.P. and Zhang, G. (2014), “Centrifuge model test study on pile reinforcement behavior of cohesive soil slopes under earthquake conditions”, *Landsides*, **11**(2), 213-223. <https://doi.org/10.1007/s10346-013-0388-2>.
- Weng, M.C., Lo, C.M., Wu, C.H. and Chuang, T.F. (2015), “Gravitational deformation mechanisms of slate slopes revealed by model tests and discrete element analysis”, *Eng. Geol.*, **189**, 116-132. <https://doi.org/10.1016/j.enggeo.2015.01.024>.
- Xu, N.X., Zhang, J.Y., Tian, H., Mei, G. and Ge, Q. (2016), “Discrete element modeling of strata and surface movement induced by mining under open-pit final slope”, *Int. J. Rock Mech. Min. Sci.*, **88**, 61-76. <https://doi.org/10.1016/j.ijrmms.2016.07.006>.
- Zou, Y.F. and Chai, H.B. (2013), *Similar Theory of Mining Subsidence and its Application*, Science China Press, Beijing, China (in Chinese).